

62(1), pp. 33-41, 2018

<https://doi.org/10.3311/PPme.11312>

Creative Commons Attribution 

András Urbán<sup>1\*</sup>, Viktor Józsa<sup>1</sup>

RESEARCH ARTICLE

Received 27 July 2017; accepted after revision 13 October 2017

## Abstract

Atomization involves mass, energy, and impulse transfer, in such a complex way that the overall process can only be described by empirical and semi-empirical correlations to date. The phenomenon of atomization is used in numerous applications, e.g., in combustion technology and metallurgy. However, many formulae are available in the literature to derive mean diameters of the spray, size distribution functions are barely discussed. Based on the measurement results performed earlier by a Phase Doppler Anemometer, twenty probability density functions were evaluated and seven are discussed in detail over the course of the present paper. The atomization pressure was varied, and characteristic regimes of the spray were measured. Interestingly, the analysis showed that not only the three most commonly used probability density functions (Nukiyama-Tanasawa, Rosin-Rammler, and Gamma) are eligible for describing the size distribution of the spray.

## Keywords

spray, curve fit, probability density function, distribution, atomization

## 1 Introduction

There are various liquid fuel systems for combustion applications in state-of-the-art technology. Industrial gas turbines operate principally with natural gas, but the combustion chamber design allows liquid fuel utilization to increase supply security [1]. In order to combust liquid fuels, the atomization conditions have to be optimized to fulfill pollutant emission standards [2]. Other practical uses of atomization are, e.g., metallurgy for powder production, two-phase flow chemical reactors, chemical separators, spray drying, painting, coating technologies, and food processing [3, 4].

Numerous studies investigated spray characterization to understand the physical background of droplet formation [5–8] bio-fuels have generated a significant interest as an alternative fuel for the future. The use of bio-fuels to fuel gas turbine seems a viable solution for the problems of decreasing fossil-fuel reserves and environmental concerns. Bio-fuels are alternative fuels, made from renewable sources and having environmental benefit. In recent years, the desire for energy independence, foreseen depletion of nonrenewable fuel resources, fluctuating petroleum fuel costs, the necessity of stimulating agriculture based economy, and the reality of climate change have created an interest in the development of bio-fuels. The application of bio-fuels in automobiles and heating applications is increasing day by day. Therefore the use of these fuels in gas turbines would extend this application to aviation field. The impact of costly petroleum-based aviation fuel on the environment is harmful. So the development of alternative fuels in aviation is important and useful. The use of liquid and gaseous fuels from biomass will help to fulfill the Kyoto targets concerning global warming emissions. In addition, to reduce exhaust emission waste gases and syngas, etc., could be used as a potential gas turbine fuel. The term bio-fuel is referred to alternative fuel which is produced from biomass. Such fuels include bio-diesel, bio-ethanol, bio-methanol, pyrolysis oil, biogas, synthetic gas (dimethyl ether. Even though several works discuss droplet dynamics in sprays generated by twin-fluid atomizers [9, 10], the atomization process is still not fully understood. Typically, representative diameters are used in the literature to

<sup>1</sup> Department of Energy Engineering, Faculty of Mechanical Engineering, Budapest University of Technology and Economics, H-1111 Budapest, Bertalan Lajos utca 4-6, Hungary

\*Corresponding author, e-mail address: [urban@energia.bme.hu](mailto:urban@energia.bme.hu)

characterize sprays [11–14]. Since spray measurement is often unfeasible or unaffordable in many circumstances, empirical formulas were extensively derived to estimate the representative diameters, especially the Sauter Mean Diameter (*SMD*,  $D_{32}$ , volume-to-surface mean diameter) of the spray [13, 15]. According to the literature, only empirical and semi-empirical correlations are available to characterize the fuel atomization even nowadays, since the droplet formation is a nearly chaotic phenomenon.

In some applications, the size distribution of the droplets in the spray plays a particularly important role. Paint sprayers in the automotive industry have a desired droplet size range below 20  $\mu\text{m}$  [16]. Classically, droplet size distribution estimation is performed in an empirical way [16]. The curves fitted to the measurement data is able to approximate the distribution of the droplet size in a wide range of operation. Among the probability density functions (PDFs), Nukiyama-Tanasawa, Rosin-Rammler, and Gamma are the most frequently used ones in atomization [14, 16–18].

The aim of the present paper, the revision of PDFs became actual for few reasons. Firstly, the currently available measurement technology far exceeds the resolution of the ones applied half-century ago when to the first systematic studies appeared to characterize spray formation. Secondly, there is an increasing number of PDFs available by time from which several have not been evaluated in atomization. In the present paper, an airblast atomizer was examined, since it has a simple geometry and used widely. Although other constructions have better efficiencies [19], however the process of atomization is well represented in this design. If the atomization velocity is low, the most unstable wave number can be calculated which allow an accurate estimate of the spray size distribution [20]. However, at elevated conditions, the superposition of several disintegration modes influence the spray evolution, reviewed by Lasheras and Hopfinger [3]. Consequently, using PDFs for determining the spray size distribution is required if not only a single phenomenon play role in atomization.

The three most popular PDFs (Nukiyama-Tanasawa, Rosin-Rammler, and Gamma) were selected in atomization research before the rapid evolution of modern measurement technology which principally uses lasers. Hence, it is time to revise the superiority of the mentioned PDFs and compete them with functions with a similar mathematical shape. Overall, this study may give a guide to fellow researchers to involve new, mathematically appropriate probability density functions for evaluating atomization measurements.

## 2 Experimental setup

Nowadays, various atomizer designs are known in the literature [13]. However, the present paper is confined to the spray analysis of a plain-jet airblast atomizer, shown in Fig. 1. The fuel jet flows in a 0.4 mm diameter line while the atomizing air

jet discharges from a concentric annulus (1.6 mm outer, 0.8 mm inner diameter). This atomizer was also examined by other researchers [2, 15, 5] due to its simple geometry and operation.

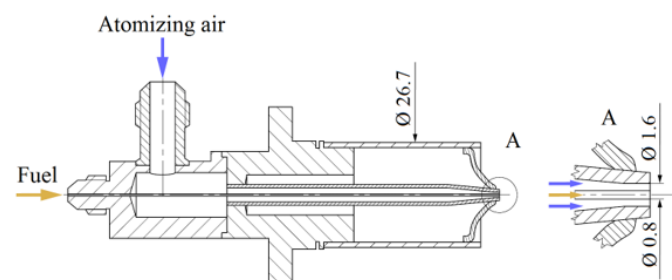


Fig. 1 Cross section of investigated atomizer.

In plain-jet airblast atomization, high-velocity air is blowing over the surface of the low-velocity liquid jet, leading to a rapid disruption of the liquid jet into droplets. Typical droplet sizes are in the range of micrometers, therefore, a Phase Doppler Anemometry (PDA) was selected for the current investigation. A 2D fiber based PDA by Dantec Dynamics was used for the measurement of velocity and droplet size. The system consists of a Spectra Physics Stabilite 2017 Argon laser, a 60X41 transmitter, a 60X81 2D 85 mm transmitting optics with 50x82 beam translator. This transmits two pairs of laser beams with wavelengths of 514.5 nm (green) and 488 nm (blue) which are used for axial and radial velocity measurement. Furthermore, a 57x50 112 mm PDA receiver optics with a spatial filter, Fiber PDA Detector and BSA P80 flow and particle processor consisted the detector system.

Focal lengths were 500 mm for both the transmitting optics and receiving optics. The half-intersection angle between the laser beams was set to  $4.303^\circ$  for separating of the beams by 38 mm. Dimensions of the measurement volume were  $d_x = 0.1166$  mm,  $d_y = 0.1162$  mm and  $d_z = 1.549$  mm. Slit size of 0.05 mm was used to reduce the  $d_z$  dimension of the measurement volume. The scattering angle was set to  $70^\circ$ .

The device measures the reflected light from droplets by a photodetector while they are bursting through the interference strip system [15, 21]. The applied software was BSA Flow Software v5.2. Below only the key parameters of the measurement setup are discussed, and the reader is redirected to [15] for more details.

The atomized liquid was standard diesel oil at 0.35 g/s mass flow rate (EN 590:2014, Viscosity: 3.5  $\text{mm}^2$ , Density: 0.825  $\text{g/cm}^3$ , Surface tension: 0.028 N/m). The measurements were performed at nine different atomization pressures ( $p_g = 0.3$ –3.1 bar) and diameters perpendicular to the axis of the atomizer at four downstream distances ( $z = 10, 15, 26.7,$  and 50 mm), summarized in Table 1.  $z = 10$  and 15 mm are in the atomizing region while  $z = 50$  mm represents the developed spray. 26.7 mm was selected since it is the cross-section of the plenum. The points at each axial distance are equidistant.

**Table 1** Sampling points of examined profiles.

Axial distance ( $z$ ) [mm]	Measurement points	Step [mm]
10	13	1
15	13	1
26.7	13	2
50	15	2

The PDA system is shown in Fig. 2. Note that the measurement area refers to a horizontal section of the spray and the measurement points lie on an investigated diameter. The limiting factors at a single measurement point were the acquisition of 20,000 samples or 15 s passed, based on previous investigations [22, 23]. The use of the time limit was required at the spray periphery.

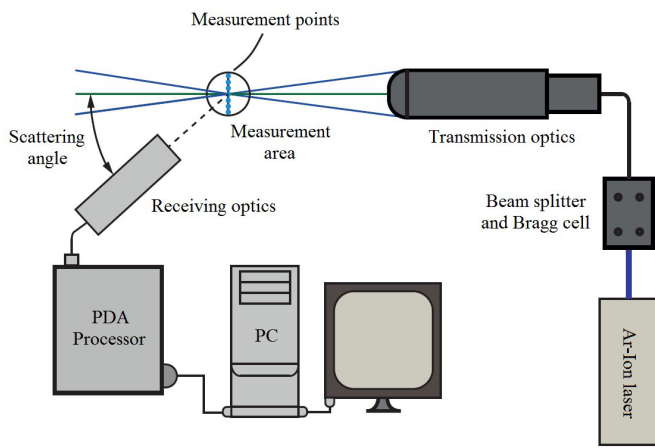


**Fig. 2** The PDA system.

The measurement system consists of air and fuel branches, shown in Fig. 3. Both branches were equipped with thermocouples and mass flow meters. In addition the atomizing air branch contained a pressure transducer. However, the air

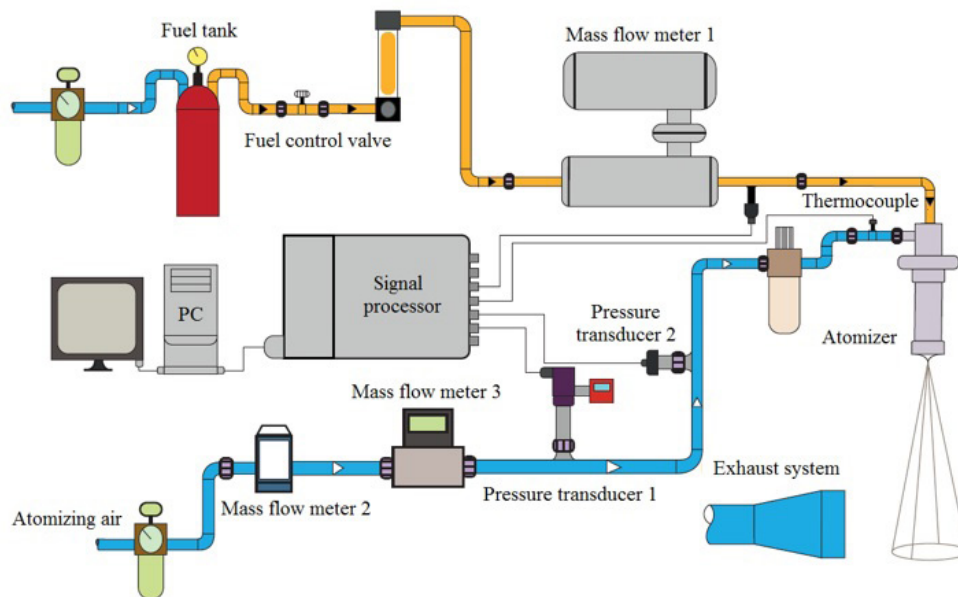


**Fig. 3** The measurement configuration.

discharge at the nozzle can be considered as adiabatic, as it was shown earlier [24], and this fact was confirmed by the mass flow meters as well. Two mass flow meters on the air side was necessary to keep the measurement error low since the first one (made by OMEGA) has a lower measurement range but higher uncertainty, shown in Table 2.

**Table 2** Instrumentation and their uncertainties.

	Instrument	Type	Comment	Uncertainty
Laser	SPECTRA PHYSICS Stabilite Series Laser Beam Specifications	Stabilite 2017 Specifications	Current mode: 17.5 A	-
	OMEGA	FMA Series	FMA-A2117	±1%
Air Side	Sierra	Smart-Trak 2	Series 100	±0.5%
	Pressure transducer 1	BD Sensor	0-35 bar; 4-20mA	±0.35%
	Pressure transducer 2	BD Sensor	0-17 bar; 4-20mA	±0.35%
Fuel Side	Fuel Tank	Old extinguishing powder	20 liter	-
	Coriolis mass flow meter – Siemens	SITRANS F C MASS 2100	Measuring the density of the fuel	≤ 0.1%
PDA	Dantec Dynamics	Fiber Flow with BSA Flow Software v5.2	Measuring the size of droplet	-
Computer	DELL Precision	T1600	-	-

The measurements were carried out at nine different atomization gauge pressures from 0.3 to 3.1 bar. The key dimensionless numbers were determined by Eqs. (1)–(3), and the results are summarized in Table 3.

$$Re_G = \frac{U_g \cdot \rho_g \cdot D_g}{\mu_g} \quad (1)$$

$$We_L = \frac{U_g^2 \cdot \rho_g \cdot D_L}{\sigma_L} \quad (2)$$

$$We_{exit} = \frac{(U_g - U_L)^2 \cdot \rho_g \cdot D_L}{\sigma_L} \quad (3)$$

where  $U_g$  is the air velocity,  $U_L$  is the liquid velocity,  $\rho_g$  is the air density,  $\sigma_L$  is the liquid surface tension,  $\mu_g$  is the air dynamic viscosity,  $D_L$  is the liquid diameter at the atomizer nozzle, and  $D_g$  is the equivalent hydraulic diameter of the annular air orifice.

Additional scaling parameters are the gas-to-liquid mass, momentum, and energy flux ratios, calculated by Eqs. (4)–(6). Here, the results have not been weighted with geometry like in [25]. In addition to the usual parameters, Mach number was also determined by Eq. (8). The results are summarized in Table 4.

$$ALR = \frac{\dot{m}_A}{\dot{m}_L}, \quad (4)$$

$$MFR = \frac{\rho_g \cdot U_g^2}{\rho_L \cdot U_L^2 \cdot D_L^2}, \quad (5)$$

$$EFR = \frac{\rho_g \cdot U_g^3}{\rho_L \cdot U_L^3 \cdot D_L^2}, \quad (6)$$

$$Ma = \frac{U_g}{a}, \quad (7)$$

where  $\dot{m}_A$  is the air mass flow,  $\dot{m}_L$  is the liquid mass flow,  $a$  is the speed of sound in the medium, the others are similar to the previous ones.

Weber number of liquid ( $We_L = 0.153$ ), and gas-to-liquid surface of atomizer orifice ( $A_{gl} = 15$ ) were independent of the atomizing pressure [20, 8]. Based on the dimensionless numbers, it is clear that the air jet dominates the flow.

### 3 Results and discussion

To visually show the atomization process and the effect of the atomization pressure, two spray images are shown in Fig. 4, captured by a Canon EOS 70D camera at 1/60 s, f/4 100mm, and ISO = 400. Note that the increasing atomizing pressure results in a narrower spread angle and a finer spray [15]. It is important to emphasize that in the case of higher atomization gauge pressures, the spray spread starts downstream the nozzle due to the supersonic conditions.

**Table 3** Dimensionless numbers by Eqs. (1)–(3) at various atomization gauge pressures.

$p_g$ [bar]	$Re_G$	$We_L$	$We_{exit}$	$We_{exit}/We_L$
0.3	9120	511041	494656	0.968
0.5	12078	774278	754080	0.974
0.7	14607	995966	973040	0.977
0.9	16881	1186495	1161461	0.979
1.1	18980	1352889	1326147	0.981
1.6	23705	1692580	1662653	0.982
2.1	27921	1957290	1925098	0.984
2.6	31786	2172164	2138243	0.984
3.1	35386	2351764	2316464	0.985

**Table 4** Gas to-liquid mass, momentum and energy flux ratios at various atomization gauge pressures.

$p_g$ [bar]	$ALR$	$MFR$	$EFR$	$Ma$
0.3	0.778	5.83	361	0.622
0.5	0.997	9.21	701	0.782
0.7	1.172	12.27	1060	0.903
0.9	1.321	15.09	1423	1.001
1.1	1.451	17.71	1783	1.084
1.6	1.725	23.54	2651	1.251
2.1	1.950	28.63	3467	1.379
2.6	2.144	33.16	4230	1.484
3.1	2.315	37.25	4945	1.573

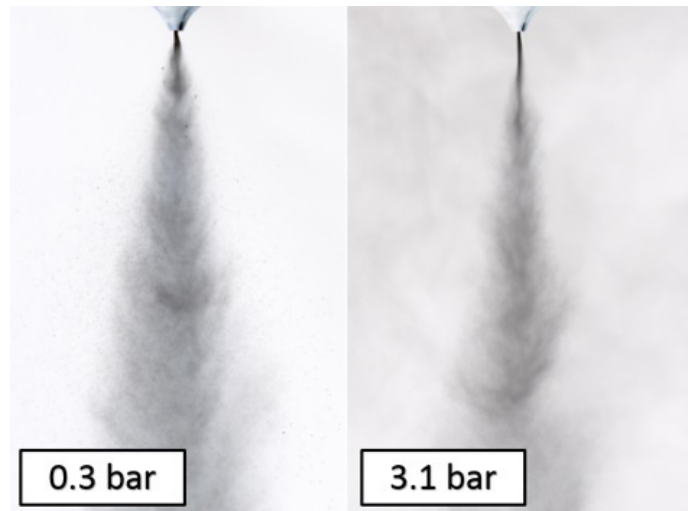


**Fig. 4** Spray structure at 0.3 bar (left) and 3.1 bar (right) atomization pressures.

In order to improve the visibility of the fast atomizing process in the neighborhood of the nozzle, a Photron FASTCAM SA-Z type 2100K-M-16GB high-speed camera was used with 1/6300000 s shutter speed. Fig. 5 shows the results at 0.3 bar and 2.4 bar atomizing gauge pressures. Based on the images, no contraction angle is observed for either sub- or supersonic flow conditions. Note that the results of the high-speed camera measurement will be discussed in a forthcoming paper.

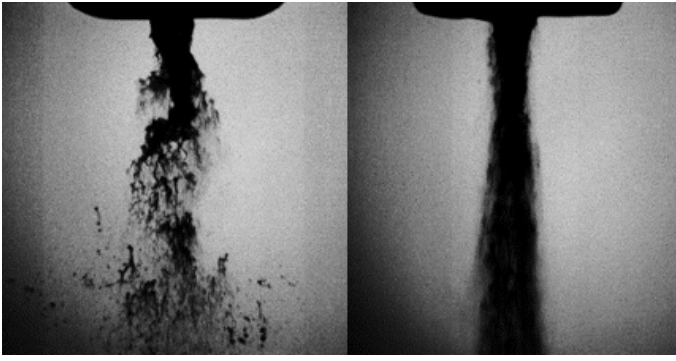


**Fig. 5** Atomization at 0.3 bar (left) and 2.4 bar (right) atomizing gauge pressures.

Numerous PDFs exist in the literature from which twenty were tested by the least squares method in MATLAB software environment. In accordance with the literature, 3 PDFs were investigated earlier [15], namely, the Nukiyama-Tanasawa (NT), the Rosin-Rammler (RR), and the Gamma ( $\Gamma$ ) [13, 26], shown by Eqs. (8)–(10). The  $\Gamma$  and RR PDFs have two parameters, while the NT has four parameters. However, the simplification of parameter  $p_{NT} = 2$  is common in the literature [16, 26] which negligibly altered the  $R^2$  value.

$$f(D)_{NT} = a_{NT} D^{p_{NT}} \cdot \exp(-b_{NT} D^{q_{NT}}) \quad (7)$$

$$f(D)_{RR} = b_{RR}/a_{RR} \cdot (D/a_{RR})^{b_{RR}-1} \cdot \exp\left[-(D/a_{RR})^{b_{RR}}\right] \quad (8)$$

$$f(D)_{\Gamma} = D^{a_{\Gamma}-1} / \left[ b_{\Gamma}^{a_{\Gamma}} \Gamma(a_{\Gamma}) \right] \cdot \exp(-D/b_{\Gamma}) \quad (9)$$

The two extreme cases by atomizing pressure are shown in Figs. 6 and 7. Within the two different setups, the closest and the furthest axial distances are presented. Tables 5 and 6 show the corresponding parameter values of the fitted functions besides their fit statistics.  $R^2$  was used for the qualitative evaluation of each density function. In addition, the sum of squared error (SSE) and root-mean-square error (RMSE) values are also presented. The SSE is the sum of the squared differences between each observation and its mean of the group while the RMSE represent how concentrated the data is around the line of the best fit. It is important to note that all the fitted PDFs were reviewed by checking their integrated value. In all cases, it is expected that this value will return close to one. The measurement data was cut at 60  $\mu\text{m}$  since the number of measured droplets over this size was negligible and notably biased the fitting procedure. Data are presented at a downstream distance,  $z = 10$  mm up to 35  $\mu\text{m}$ , and at  $z = 50$  mm the upper limit was set to 25  $\mu\text{m}$ . However, the fit procedure considered all the droplets up to 60  $\mu\text{m}$ . All the used measurement points were located at the axis of the atomizer ( $r = 0$  mm).

At  $z = 50$  mm, the  $R^2$  of RR PDF decreases compared to that of  $z = 10$  mm. However, the  $R^2$  of the NT and  $\Gamma$  PDFs minimally altered at these measurement points.

**Table 5** Fit of the common PDFs at  $p_g = 0.3$  bar,  $r = 0$  mm,  $z = 10$  and 50 mm.

$z$	10 mm			50 mm		
	NT	RR	$\Gamma$	NT	RR	$\Gamma$
$a$	217.8	9.71	4.38	375.45	7.35	2.57
$b$	12.23	2.32	2.08	9.58	1.74	2.66
$p$	8.55	-	-	5.56	-	-
$q$	0.36	-	-	0.36	-	-
SSE (%)	0.05	0.13	0.11	0.11	0.42	0.24
$R^2$ (%)	98.95	97.59	97.89	98	92.47	95.79
RMSE (%)	0.34	0.51	0.48	0.49	0.94	0.7
Integral	1	1	1	1	0.99	1

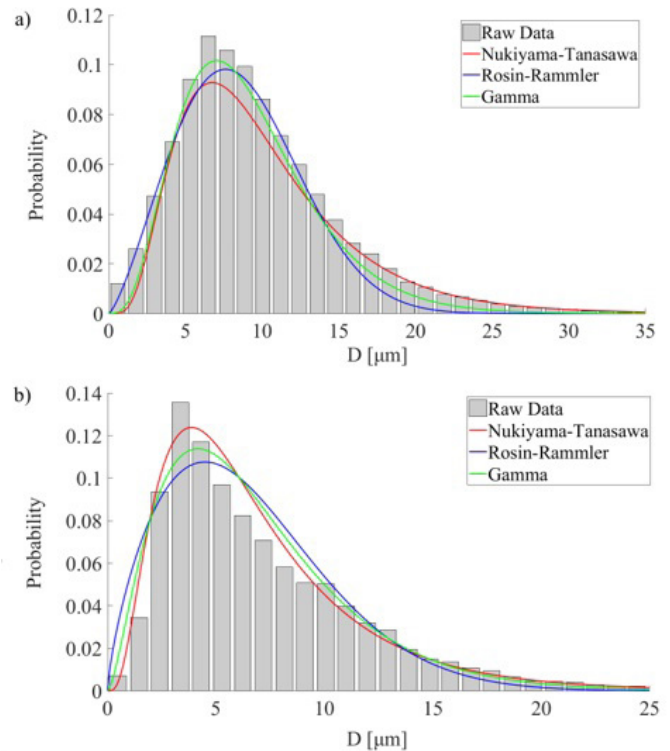


**Fig. 6** Three commonly used fitted PDFs at  $p_g = 0.3$  bar. a)  $z = 10$ , b) 50 mm.

The results shown quantitatively in Table 6 are presented qualitatively in Fig. 7. It is obvious that the droplet diameters are shifted to the lower values at  $z = 50$  mm which results in higher probability of smaller droplets in the spray and a narrower size distribution. At  $z = 10$  mm, the atomization is not yet complete and larger liquid fractions are present. Note that the PDA system registers only the closely spherical droplets, therefore, the ligaments and other structures are rejected, and the measurement data contains limited information about these fluid packets. Despite the ongoing atomization in the near field region of the atomizer which resulted in obviously worse data quality, the  $R^2$  values were nearly the same at each axial distance and atomization pressure. However, SSE and RMSE values show an outstanding quality because they remain below 1% for each point. Only the RR PDF could not fit the narrower distribution.

This is also observed in the decrease of  $R^2$  and the growth of  $SSE$  and  $RMSE$ . The  $RMSE$  value, in this case, is almost 1%. Furthermore, it can be observed that there are larger  $R^2$  values in general for higher atomization pressures. Hence, it can be stated that the quality of fit depends on the applied atomizing pressure and the widely applied RR PDF does not seem a superior choice over the others [15, 16]. Note that this PDF was originally used for size characterization of coal particles after milling [13].

**Table 6** Fit of the common PDFs at  $p_g = 3.1$  bar,  $r = 0$  mm,  $z = 10$  and 50 mm.

z	10 mm			50 mm		
	NT	RR	$\Gamma$	NT	RR	$\Gamma$
a	0.06	6.98	3.05	0.11	5.26	6.93
b	0.01	1.98	2.16	2.26	2.95	0.71
p	0.62	-	-	5.43	-	-
q	2.49	-	-	0.78	-	-
SSE (%)	0.04	0.15	0.29	0.21	0.81	0.72
$R^2$ (%)	99.5	97.95	95.91	97.06	95.12	95.23
RMSE (%)	0.28	0.55	0.78	0.67	1.32	1.21
Integral	1.01	1	1	1	1	1

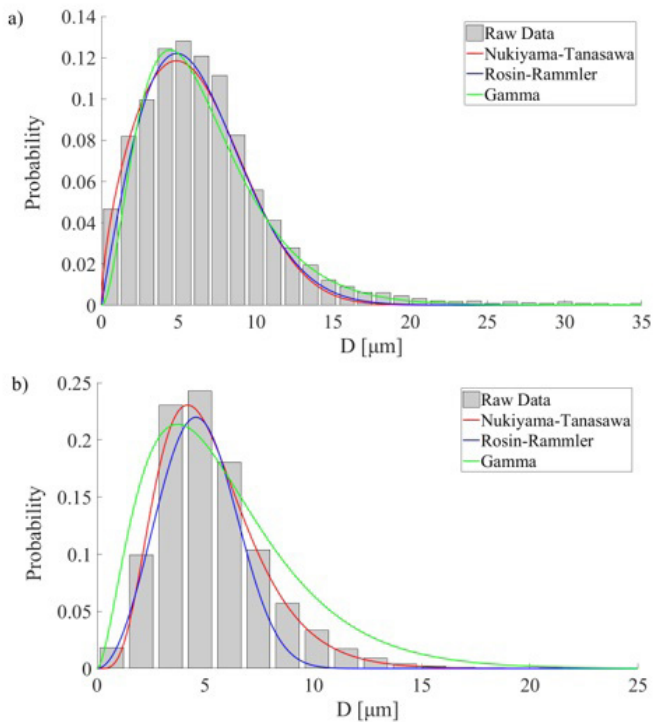


**Fig. 7** Fit of the common PDFs at  $p_g = 3.1$  bar. a)  $z = 10$ , b) 50 mm.

In the followings, four additional probability density functions are analyzed. The reasons for rejecting the other thirteen built-in PDFs in MATLAB are the following. Firstly, the PDF must be unimodal. Secondly, the maximum value of the fitted function was located at a larger  $D$  that does not correspond to reality, and they were characterized by too low  $R^2$  values. The failed PDFs are Binomial, Negative Binomial, Poisson, Loglogistic, Beta, and Birnbaum-Saunders. Thirdly, there were

functions whose fitting did not provide a solution: Logistic, Burr Type XII, Generalized Pareto, Chi-Square. There were also PDFs for which the distribution curve was negative: t Location-Scale, Student's t, Rician. It is important to mention that those functions that contain a factorial expression are unable to describe the present distributions.

As a result of this study, it can be seen that the three most commonly used density functions have proved to be adequate for global spray characterization. However, it is worth examining additional functions that may also be suitable. Based on preliminary studies, only those functions are analyzed in detail which are outstanding and approximate to the goodness of fit of above-presented examples.

In the followings, the fit four additional PDFs to the same data are discussed which meet the above-listed requirements. The alternative functions were the Rayleigh (Ra), Nakagami (Na), Normal (No) and Lognormal (Lo). The formulae of these functions are described by Eqs. (11)–(14). Na, No, and Lo have two parameters, while Ra has a single parameter. Figs. 8 and 9 show the qualitative results of the fit while the parameter values are summarized in Tables 7 and 8.

$$f(D)_{Ra} = (D/a_{Ra}^2) \cdot \exp\left[-D^2/(2 \cdot a_{Ra}^2)\right] \quad (11)$$

$$f(D)_{Na} = 2 \cdot (a_{Na}/b_{Na})^{a_{Na}} \cdot \left[\frac{1}{\Gamma(a_{Na})}\right] \cdot D^{(2 \cdot a_{Na} - 1)} \cdot \exp\left(-a_{Na} \cdot D^2/b_{Na}\right) \quad (12)$$

$$f(D)_{No} = 1/(a_{No} \cdot \sqrt{2 \cdot \pi}) \cdot \exp\left[-(D - b_{No})^2/2 \cdot a_{No}^2\right] \quad (13)$$

$$f(D)_{Lo} = (1/(D \cdot a_{Lo} \cdot \sqrt{2 \cdot \pi})) \cdot \exp\left(-(\ln D - b_{Lo})^2/2 \cdot \sigma_{Lo}^2\right) \quad (14)$$

Here, a clear decrease in the fit quality between  $z = 10$  and 50 mm is visible. Lognormal is an exception which provides a higher  $R^2$  value at  $z = 50$  mm. Although the  $R^2$  values can be treated as outstanding, the integral values show slightly worse results. This is particularly the case for Ra and No PDFs. It is also worth to mention that the  $R^2$  of the Ra PDF dramatically decreases by increasing the atomization pressure. However, in the case of Na PDF, this is exactly the inverse. For these functions, the  $RMSE$  and  $SSE$  values have already exceeded 1% in several cases. This is particularly true at  $z = 50$  mm where the previously described phenomena prevail meaning that the narrower distribution is harder to trace with this PDF type. In addition, significant deterioration is observed depending on the distance from the spray nozzle in case of the No PDF. However, it is clear that Ra PDF cannot follow the sudden change caused by the high atomization pressure. Therefore, this density function is only acceptable for low pressures since it is not able to characterize the global spray across the entire operating range.

**Table 7** Results of the four alternative fitted PDFs at  $p_g = 0.3$  bar,  $r = 0$  mm,  $z = 10$  and 50 mm

$z$	10 mm				50 mm			
	Ra	Na	No	Lo	Ra	Na	No	Lo
PDFs								
$a$	6.95	1.29	3.96	0.5	4.99	0.85	3.47	0.69
$b$	-	91.8	8.09	2.15	-	54.8	5.74	1.81
SSE (%)	0.23	0.11	0.21	0.18	0.58	0.49	0.72	0.09
$R^2$ (%)	95.7	97.8	96	96.6	89.7	91.4	87.2	98.4
RMSE (%)	0.68	0.48	0.66	0.61	1.09	1.01	8.68	0.43
Integral	1	1	0.99	1	1	0.99	0.97	1

**Table 8** Results of four alternative fitted PDFs at  $p_g = 3.1$  bar,  $r = 0$  mm,  $z = 10$  and 50 mm

$z$	10 mm				50 mm			
	Ra	Na	No	Lo	Ra	Na	No	Lo
PDFs								
$a$	4.94	0.96	3.25	0.6	3.81	1.95	1.75	0.39
$b$	-	49	5.56	1.81	-	26.2	4.63	1.55
SSE (%)	0.15	0.14	0.19	0.54	2.1	0.71	0.92	0.86
$R^2$ (%)	97.9	98	97.3	92.3	86.5	95.6	94.2	95.1
RMSE (%)	0.55	0.54	0.63	1.06	2.1	1.23	1.37	1.3
Integral	1	1	0.97	1	0.99	1	1	1

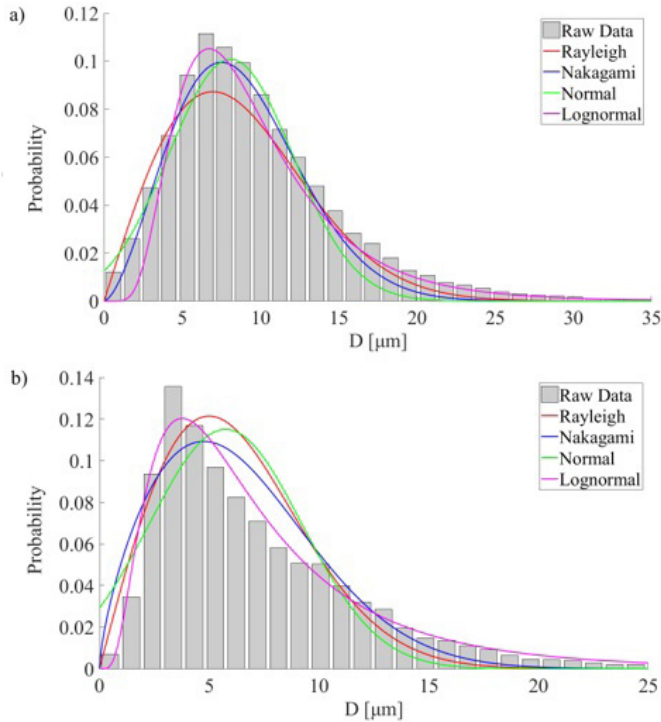


**Fig. 8** Four alternative fitted PDFs at  $p_g = 0.3$  bar. a)  $z = 10$ , b) 50 mm.

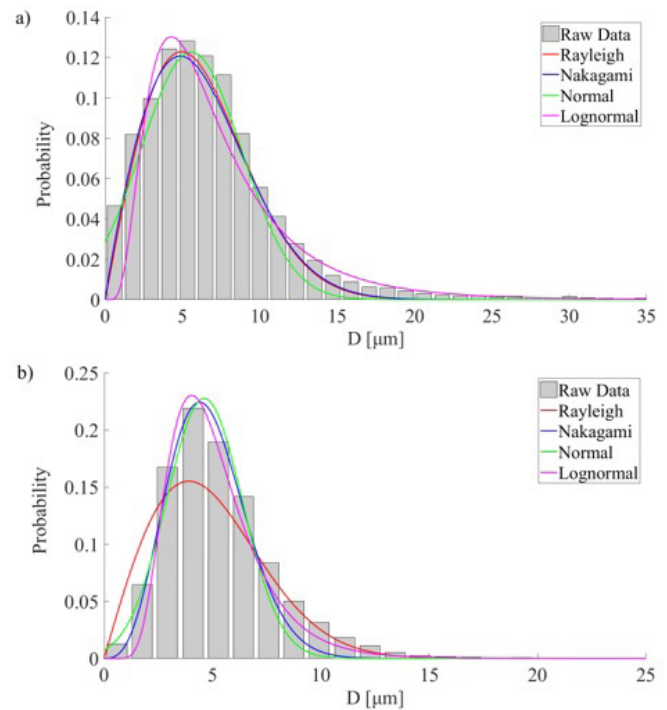


**Fig. 9** Four alternative fitted PDFs at  $p_g = 3.1$  bar. a)  $z = 10$ , b) 50 mm.

The analysis described above was also performed for the complete spray. Thus, globally statements can be made about the fit of the PDFs. Three and four parametric version of Nukiyama-Tanasawa were evaluated since there are papers where the  $p = 2$  simplification was applied [17]. In order to minimize the error, measurement points with insufficient data which means less than 20,000 samples in 15 s were neglected to achieve a statistically more significant fit. These peripheral regions showed varying and irregular droplet distributions. Practically, it means that the furthest planes ( $z = 26.7$  and 50 mm) from the nozzle was calculated for the range of  $-10 \text{ mm} < r < 10 \text{ mm}$ . Meanwhile, the nearest planes ( $z = 10$  and 15 mm) evaluated at  $-6 \text{ mm} < r < 6 \text{ mm}$ . The results are presented in Figs. 10–13. All figures include a limitation of  $R^2$  of unity since there are some cases where the error bars exceed this value. Nevertheless, it is mathematically impossible to exceed one.

At  $z = 50$  mm, Na, No, and Lo PDFs were able to provide a similar quality of fit compared to the commonly used ones.

In this section, NT (3) and NT (4) resulted in the best fits at each axial distance. Nevertheless, the three and four-parametric probability density functions should be treated with caution because of the problem of overfitting. By getting closer to the nozzle, the average results getting worse and the results became more stochastic. Because of the higher velocity, the spray becomes more monochromatic, so a better fit is expected from the functions at the same atomizer inlet conditions, which is supported by the results. However, it is important to note that the PDA results at  $z = 10$  and 15 mm are only a rough estimate of the droplet size due to the physical limitations of the PDA system.

#### 4 Conclusions

Probability density functions (PDFs) which are and are not commonly used in the field of atomization were evaluated, using a plain-jet airblast atomizer. The derived histograms of size distribution were normalized then various PDFs were fitted on them. The fit was shown both qualitatively by images

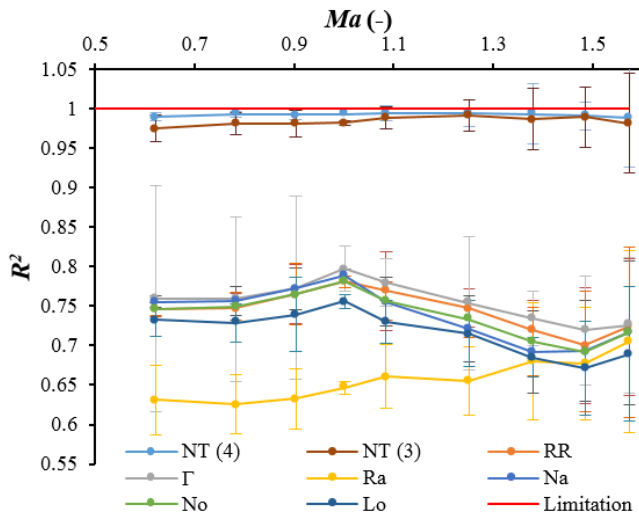


Fig. 10 The averaged coefficient of determination of fits in case of all the investigated PDFs at  $z = 10$  mm.

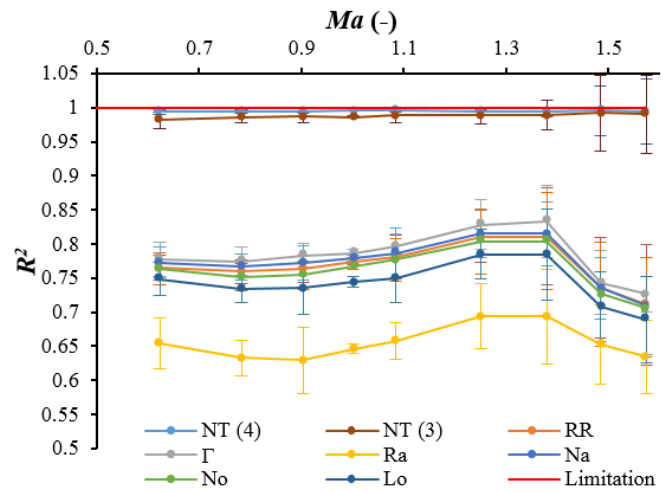


Fig. 11 The averaged coefficient of determination of fits in case of all the investigated PDFs at  $z = 15$  mm.

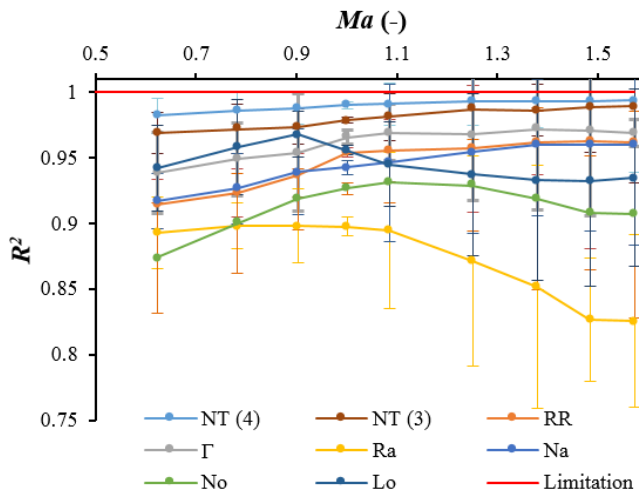


Fig. 12 The averaged coefficient of determination of fits in case of all the investigated PDFs at  $z = 26.7$  mm.

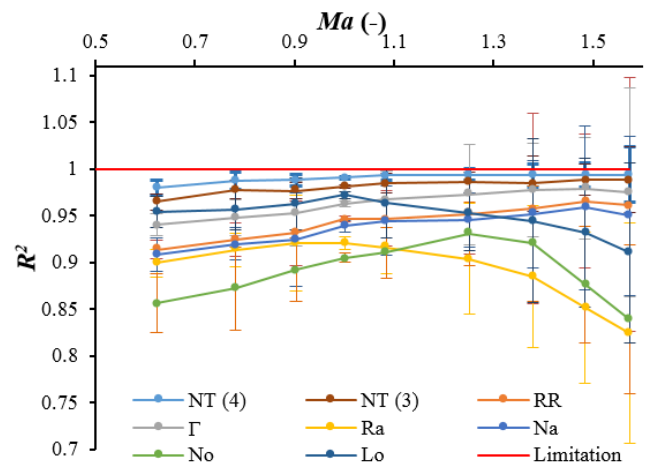


Fig. 13 The averaged coefficient of determination of fits in case of all the investigated PDFs at  $z = 50$  mm.

and quantitatively by evaluating the  $R^2$ , sum of squared error ( $SSE$ ), and root-mean-square error ( $RMSE$ ).

Note that the three widespread PDFs (Nukiyama-Tanasawa, Rosin-Rammler, and Gamma) were selected in atomization research before the rapid evolution of modern measurement technology which principally uses lasers. Hence, it was time to revise the expected superiority of the mentioned PDFs and compete them with functions with a similar mathematical shape. Based on the results, four PDFs were found to be also suitable for droplet size distribution characterization. They are the Rayleigh (Ra), Nakagami (Na), Normal (No), and Lognormal (Lo) PDFs while thirteen other PDFs were discarded.

Nevertheless, some of the four additional PDFs are limited to certain operating conditions and remarkably outperformed by the others. As for the mathematical requirements of a suitable PDF:

- It should be unimodal.
- It should include an exponential term.

- It has to have at least two parameters.
- The value of the PDF cannot be negative.

Overall, this study may give guide to fellow researchers to involve new, mathematically appropriate probability density functions for evaluating atomization measurements.

### Acknowledgements

This paper was supported by the Visegrád 3-111-0027 Strategic Support, V4 Green Energy Platform and the János Bolyai Research Scholarship of the Hungarian Academy of Sciences.

### Nomenclature

$D$	[ $\mu\text{m}$ ]	Droplet diameter
$SMD$	[ $\mu\text{m}$ ]	Sauter Mean Diameter
$z$	[ $\mu\text{m}$ ]	Distance from the nozzle

$r$	[mm]	Radial distance from the center
$p_g$	[bar]	Atomization gauge pressure
$R^2$	[-]	Coefficient of determination
$SSE$	[-]	Sum of squared error
$RMSE$	[-]	Root-mean-square error

## Abbreviations

NT	Nukiyama-Tanasawa
RR	Rosin-Rammler
$\Gamma$	Gamma
Ra	Rayleigh
Na	Nakagami
No	Normal
Lo	Lognormal

## References

- [1] Kyprianidis, K. G., Skvaril, J. "Developments in Combustion Technology." InTech, Cranfield, 2016.  
<https://doi.org/10.5772/61418>
- [2] Kun-Balog, A., Sztankó, K. "Reduction of pollutant emissions from a rapeseed oil fired micro gas turbine burner." *Fuel Processing Technology*. 134, pp. 352–359. 2015.  
<https://doi.org/10.1016/j.fuproc.2015.02.017>
- [3] Lasheras, J. C., Hopfinger, E. J. "Liquid jet instability and atomization in a coaxial gas stream." *Annual Review of Fluid Mechanics*. 32, pp. 275–308. 2000.  
<https://doi.org/10.1146/annurev.fluid.32.1.275>
- [4] Józsa, V. "Numerical investigation of a plain jet air blast atomiser." In: *Proceedings of Conference on Modelling Fluid Flow (CMFF'15)* (p. 7). Budapest. 2015.
- [5] Bolszo, C. D. "Investigation of Atomization, Mixing and Pollutant Emissions for a Microturbine Engine." *The UCI Undergraduate Research Journal*. (2), pp. 13–22. 2005.
- [6] Gupta, K. K., Rehman, A., Sarviya, R. M. "Bio-fuels for the gas turbine: A review." *Renewable and Sustainable Energy Reviews*. 14(9), pp. 2946–2955. 2010.  
<https://doi.org/10.1016/j.rser.2010.07.025>
- [7] Lasheras, J. C., Villermaux, E., Hopfinger, E. J. "Break-up and atomization of a round water jet by a high-speed annular air jet." *Journal of Fluid Mechanics*. 357, pp. 351–379. 1998.  
<https://doi.org/10.1017/S0022112097008070>
- [8] Varga, C. M., Lasheras, J. C., Hopfinger, E. J. "Initial breakup of a small-diameter liquid jet by a high-speed gas stream." *Journal of Fluid Mechanics*. 497, pp. 405–434. 2003.  
<https://doi.org/10.1017/S0022112003006724>
- [9] Durdina, L., Jedelsky, J., Jicha, M. "Investigation and comparison of spray characteristics of pressure-swirl atomizers for a small-sized aircraft turbine engine." *International Journal of Heat and Mass Transfer*. 78, pp. 892–900. 2014.  
<https://doi.org/10.1016/j.ijheatmasstransfer.2014.07.066>
- [10] Kourmatzis, A., Pham, P. X., Masri, A. R. "Air assisted atomization and spray density characterization of ethanol and a range of biodiesels." *Fuel*. 108, pp. 758–770. 2013.  
<https://doi.org/10.1016/j.fuel.2013.01.069>
- [11] Li, Z., Wu, Y., Yang, H., Cai, C., Zhang, H., Hashiguchi, K., Takeno, K., Lu, J. "Effect of liquid viscosity on atomization in an internal-mixing twin-fluid atomizer." *Fuel*. 103, pp. 486–494. 2013.  
<https://doi.org/10.1016/j.fuel.2012.06.097>
- [12] Li, Z., Wu, Y., Cai, C., Zhang, H., Gong, Y., Takeno, K., Hashiguchi, K., Lu, J. "Mixing and atomization characteristics in an internal-mixing twin-fluid atomizer." *Fuel*. 97, pp. 306–314. 2012.  
<https://doi.org/10.1016/j.fuel.2012.03.006>
- [13] Lefebvre, A. H. "Atomization and Sprays." Hemisphere Publishing Corporation. 1989.
- [14] Nukiyama, S., Tanasawa, Y. "Experiments on the atomization of liquids in an airstream." *Transactions of the Japan Society of Mechanical Engineers*. 5, pp. 68–75. 1939.
- [15] Urbán, A., Zaremba, M., Malý, M., Józsa, V., Jedelský, J. "Droplet dynamics and size characterization of high-velocity airblast atomization." *International Journal of Multiphase Flow*. 95, pp. 1–11. 2017.  
<https://doi.org/10.1016/j.ijmultiphaseflow.2017.02.001>
- [16] Babinsky, E., Sojka, P. E. "Modeling drop size distributions." *Progress in Energy and Combustion Science*. 28(4), pp. 303–329. 2002.  
[https://doi.org/10.1016/S0360-1285\(02\)00004-7](https://doi.org/10.1016/S0360-1285(02)00004-7)
- [17] Li, X., Tankin, R. S. "Droplet size distribution: a derivation of a Nukiyama-Tanasawa type distribution function." *Combustion Science Technology*. 56, pp. 65–76. 1987.  
<https://doi.org/10.1080/00102208708947081>
- [18] Mugele, R. A., Evans, H. D. "Droplet size distributions in sprays." *Industrial & Engineering Chemistry*. 43(6), pp. 1317–1324. 1951.  
<https://doi.org/10.1021/ie50498a023>
- [19] Jedelsky, J., Jicha, M. "Energy considerations in spraying process of a spill-return pressure-swirl atomizer." *Applied Energy*. 132, pp. 485–495. 2014.  
<https://doi.org/10.1016/j.apenergy.2014.07.042>
- [20] Kourmatzis A., Masri A. R. "Air-assisted atomization of liquid jets in varying levels of turbulence." *Journal of Fluid Mechanics*. 764, pp. 95–132. 2014.  
<https://doi.org/10.1017/jfm.2014.700>
- [21] Dantec Dynamics. "Integrated solutions in Particle Dynamics Analysis." *Nova Instruments*, pp. 2–4. (n.d.)
- [22] Jedelský, J., Zaremba, M., Malý, M., Jicha, M. "Characteristics of droplet motion in effervescent sprays." *EPJ Web of Conferences*. 67, pp. Article 2050. 2014.  
<https://doi.org/10.1051/epjconf/20146702050>
- [23] Zaremba, M., Milkvik, M., Malý, M., Jedelský, J., Jicha, M. "Evaluation of Steadiness and Drop Size Distribution in Sprays Generated by Different Twin-Fluid Atomizers." *EPJ Web of Conferences*. 92, Article 02118, 2015.  
<https://doi.org/10.1051/epjconf/20159202118>
- [24] Józsa, V., Csemány, D. "Evaporation of Renewable Fuels in a Lean Pre-mixed Prevaporized Burner." *Periodica Polytechnica Mechanical Engineering*. 60(2), pp. 82–88. 2016.  
<https://doi.org/10.3311/PPme.8564>
- [25] Engelbert, C., Hardalupas, Y., Whitelaw, J. H. "Breakup Phenomena in Coaxial Airblast Atomizers." *Proceedings of the Royal Society A*. 451, pp. 189–229. 1995.  
<https://doi.org/10.1098/rspa.1995.0123>
- [26] Liu, H. F., Gong, X., Li, W. F., Wang, F. C., Yu, Z. H. "Prediction of droplet size distribution in sprays of prefilming air-blast atomizers." *Chemical Engineering Science*. 61(6), pp. 1741–1747. 2006.  
<https://doi.org/10.1016/j.ces.2005.10.012>